Supporting Information

Constraints on aerosol nitrate photolysis as a potential source of HONO and NO_x

Paul S. Romer[a], Paul J. Wooldridge[a], John D. Crounse[b], Michelle J. Kim[b], Paul O. Wennberg[b,c], Jack E. Dibb[d], Eric Scheuer[d], Donald R. Blake[e], Simone Meinardi[e], Alexandra L. Brosius[f], Alexander B. Thames[f], David O. Miller[f], William H. Brune[f], Samuel R. Hall[g], Thomas B. Ryerson[h], and Ronald C. Cohen[a,i]

[a] Department of Chemistry, University of California Berkeley, Berkeley, CA 94720, USA.
[b] Division of Geological and Planetary Sciences, California Institute of Technology, Pasadena, CA 91125, USA.
[c] Division of Engineering and Applied Science, California Institute of Technology, Pasadena, CA 91125, USA.
[d] Institute for the Study of Earth, Oceans, and Space, University of New Hampshire, Durham, NH 03824, USA.
[e] Department of Chemistry, University of California Irvine, Irvine, CA 92697, USA.
[f] Department of Meteorology and Atmospheric Science, The Pennsylvania State University, University Park, PA 16802, USA.
[g] Atmospheric Chemistry Observations and Modeling Laboratory, NCAR, Boulder, CO 80301, USA.
[h] Chemical Sciences Division, NOAA Earth System Research Laboratory, Boulder, CO 80305, USA.
[i] Department of Earth and Planetary Sciences, University of California Berkeley, Berkeley, CA 94720, USA.

Contents

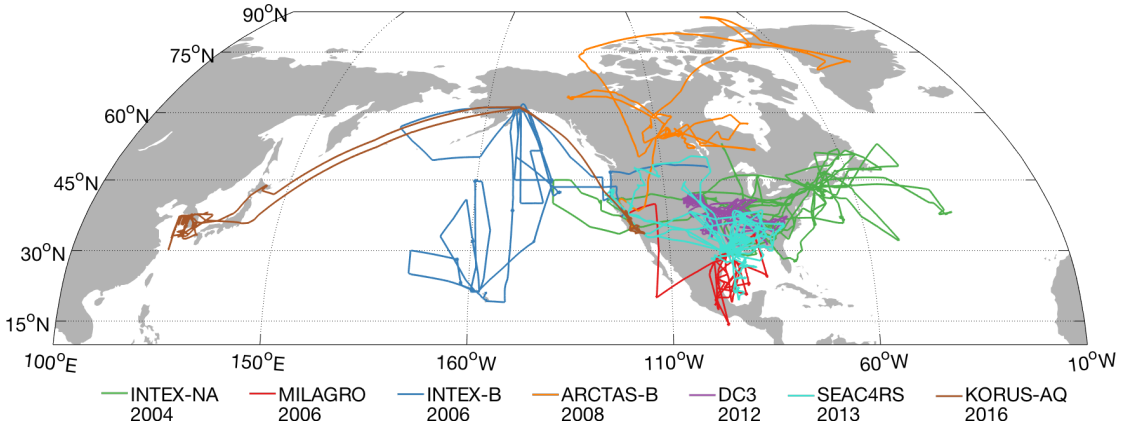

Figure S1: Map of all measurements taken on all 7 campaigns used in the extended analysis. The first phase of ARCTAS deployment (ARCTAS-A) was not included because conditions in the springtime Arctic (low light, high halogens) make it difficult to compare against other spring/summertime measurements.

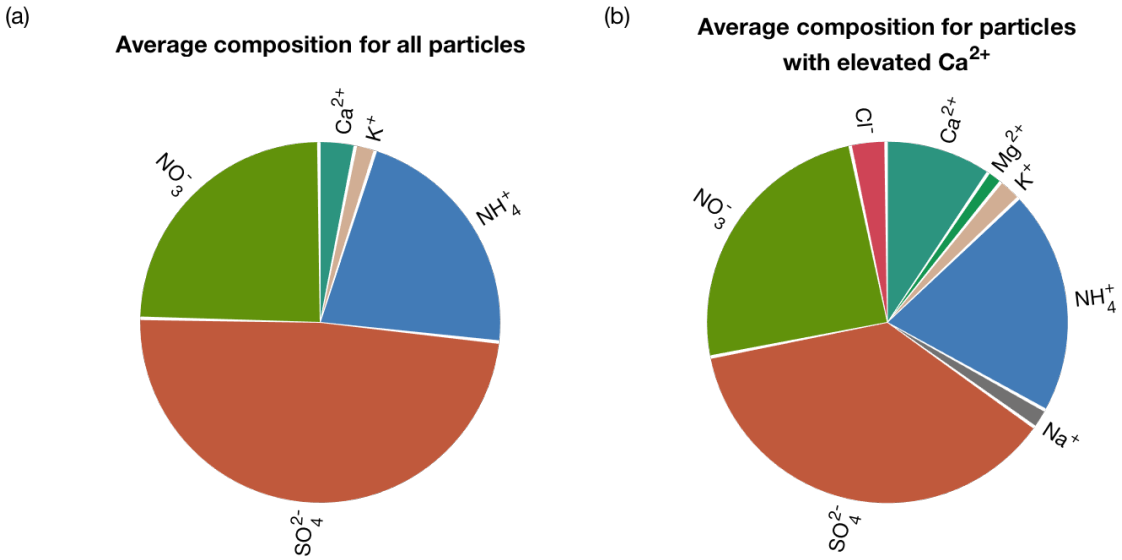

Figure S2: Average inorganic mass composition measured by SAGA in the boundary layer over the Yellow Sea for all filter samples (Panel a) and samples with over 5% mass composed of Ca^{2+} ions (Panel b).

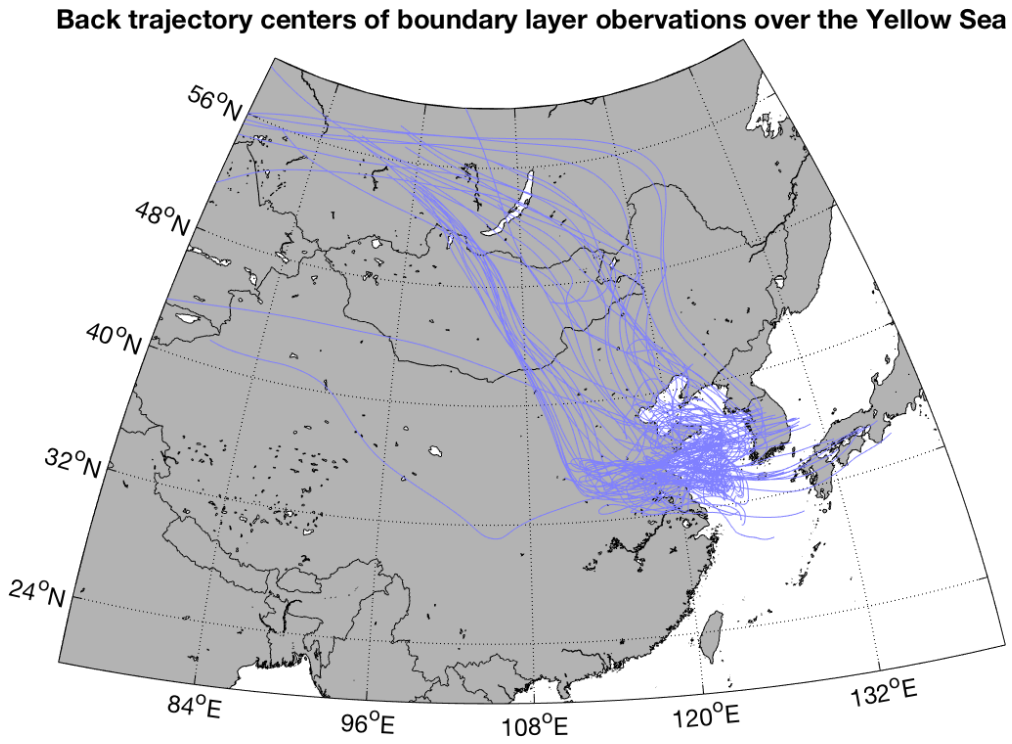

Figure S3: Back trajectories of airmasses sampled by the DC-8 in the boundary layer over the Yellow Sea calculated using FLEXPART driven by NCEP GFS analyses.

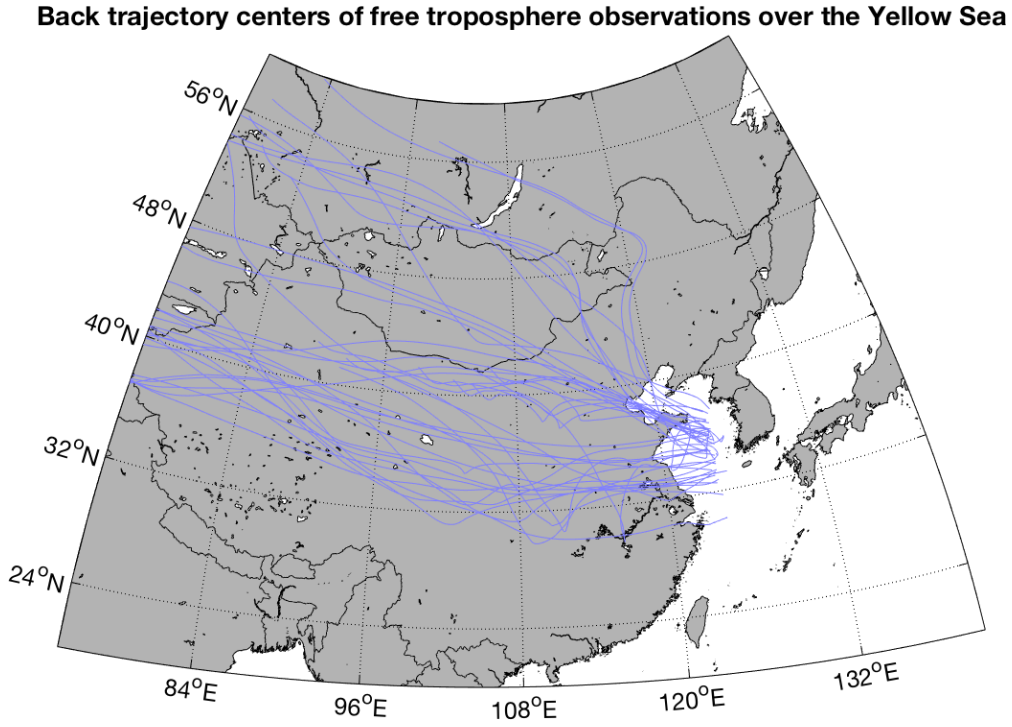

Figure S4: Back trajectories of airmasses sampled by the DC-8 in the free troposphere over the Yellow Sea calculated using FLEXPART driven by NCEP GFS analyses.

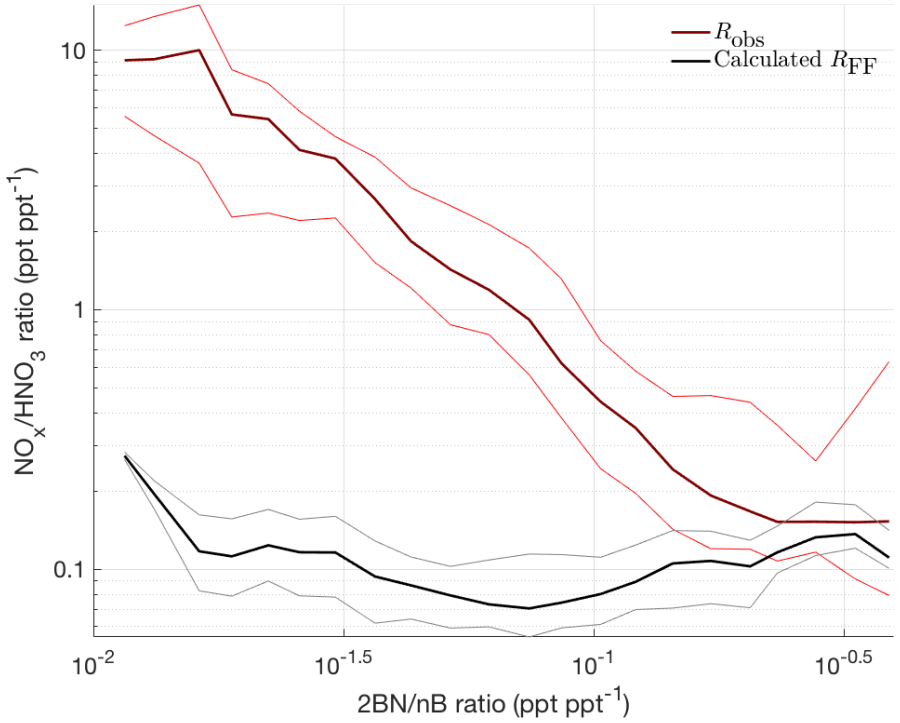

Figure S5: Evolution of the observed NO_x/HNO_3 ratio (red) and the calculated far-field ratio (black) as a function of the 2-Butyl Nitrate to n-butane ratio for all boundary-layer observations during KORUS-AQ. For both quantities, the thick line shows the binned median, and the thin lines show the binned inter-quartile range. R_{FF} is calculated assuming $EF = 10$ and using the best-guess estimates from Table S1.

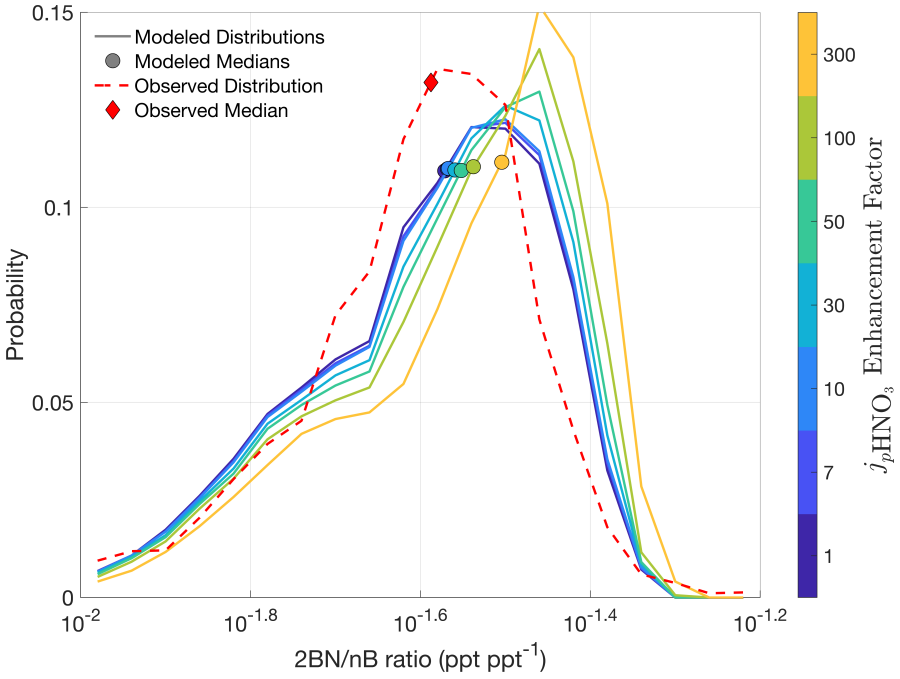

Figure S6: Modeled and observed distribution of 2BN/nB ratios over the Yellow Sea. The modeled distribution includes all daytime model points between 0 and 3 days after model initialization.

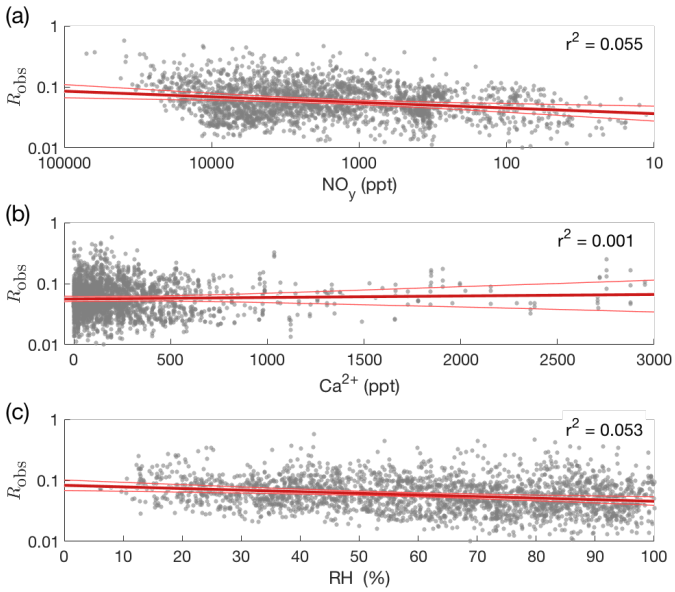

Figure S7: R_{obs} in highly-aged airmasses as a function of total NO_y (Panel a), Ca^{2+} (Panel b), and relative humidity (Panel c). Note the reversed x-axis in Panel a, so that moving to the right on all panels is expected to correspond to an increase in nitrate photolysis rate and therefore an increase in R_{obs}. The thick red line represents a linear fit to all data points; the thin red lines show the error in the fit calculated by bootstrap sampling.

Table S1: Parameters used in the calculation of R_{FF}.

Parameter	Low-End	Best-Guess	High-End
Cl_Y (ppt)	7.0	18	36
Br_Y (ppt)	2.5	3.5	7.0
I_Y (ppt)	2.5	5.5	11
γ_{ClONO_2}	0.01	0.10	0.30
γ_{BrONO_2}	0.02	0.10	0.80
γ_{IONO_2}	0.02	0.10	0.80
γ_{RONO_2}	0.001	0.002	0.010
MW_{RONO_2} (kg)	0.120	0.120	0.120
v_{dep,HNO_3} (cm s^{-1})[a]	1	2	4

[a] Gas-phase only, daytime average.

Table S2: Parameters used for modeling of plumes over the Yellow Sea. Median values were chosen to match best-guess estimates in the calculation of R_{FF}. The 5^{th} and 95^{th} percentiles were set to best match the low-end and high-end estimates using either a normal or a log-normal distribution.

Parameter	Median Value	5^{th}–95^{th} percentiles
Pressure (mbar)	960	880–990
Temperature (K)	291	287–296
RelativeHumidity (%)	47	21–80
Altitude (km)	0.46	0.16–1.2
Latitude (°N)	20	10–30
HNO_3 Gas-Phase Fraction	0.51	0.12–0.88
Aerosol Surface Area (μm^2 cm^{-3})	38	10–134
k_{dil} (s^{-1})	1.7e-05	1.1e-05–2.3e-05
v_{dep,HNO_3} (cm s^{-1})[a]	2.0	1.1–4.0
γ_{ClONO_2}	0.10	0.017–0.60
γ_{BrONO_2}	0.10	0.015–0.68
γ_{IONO_2}	0.10	0.015–0.68
γ_{RONO_2}	0.005	0.003–0.009
$\gamma_{N_2O_5}$	0.014	0.007–0.039
Br_Y (ppt)	3.5	2.0–6.0
Cl_Y (ppt)	18	7.7–42
I_Y (ppt)	5.5	2.5–12

[a] Gas-phase only, daytime average.

Table S3: Initial concentrations used for modeling of plumes over the Yellow Sea.

Species	Median Concentration	5^{th}–95^{th} percentiles
O_3 (ppb)	33	6–77
NO (ppb)	18	4–56
NO_2 (ppb)	15	3–42
HNO_3 (ppb)	4.6	1.1–13
PAN (ppb)	2.1	0.7–5.1
Methane (ppb)	2050	1920–2240
CO (ppb)	320	180–540
Ethane (ppb)	3.5	2.0–7.2
Ethene (ppb)	1.1	0.34–19
Propane (ppb)	2.9	1.1–15
Propene (ppb)	0.21	0.05–5.5
n-Butane (ppb)	1.5	0.5–5.6
2-Butyl Nitrate (ppb)	0.026	0.011–0.072
n-Pentane (ppb)	0.69	0.18–2.7
n-Hexane (ppb)	0.37	0.07–5.7
Toluene (ppb)	1.8	0.32–6.3
m-Xylene (ppb)	0.55	0.14–2.4
Isoprene (ppb)	0.3	0.04–0.6
α-Pinene (ppb)	0.016	0.004–0.054
Methanol (ppb)	19	8–42
Acetaldehyde (ppb)	2.5	0.7–7.1
Formaldehyde (ppb)	4.6	1.8–14
Additional VOCR (s^{-1})	1.4	1.4–1.4

Table S4: Background concentrations used for modeling of plumes over the Yellow Sea.

Species	Median Concentration	5^{th}–95^{th} percentiles
O_3 (ppb)	99	79–120
NO_x (ppb)[a]	0.14	0.07–0.20
HNO_3 (ppb)	2.6	1.3–3.4
PAN (ppb)	0.6	0.3–1.4
Methane (ppb)	1960	1930–2020
CO (ppb)	194	147–309
Ethane (ppb)	2.78	2.12–3.18
Ethene (ppb)	0.013	0.006–0.019
Propane (ppb)	0.80	0.44–1.0
Propene (ppb)	0.017	0.015–0.019
n-Butane (ppb)	0.096	0.07–0.265
2-Butyl Nitrate (ppb)	0.025	0.016–0.029
n-Pentane (ppb)	0.02	0.008–0.07
n-Hexane (ppb)	0.01	0.004–0.05
Toluene (ppb)	0.005	0.002–0.17
m-Xylene (ppb)	0.012	0.006–0.015
Isoprene (ppb)	0.01	0.002–0.04
α-Pinene (ppb)	0	0–0
Methanol (ppb)	6.7	5.0–11.2
Acetaldehyde (ppb)	0.33	0.25–1.2
Formaldehyde (ppb)	0.506	0.35–3.1

[a] The partitioning of background NO_x between NO and NO_2 was assumed to match the instantaneous partitioning in the model.

Eigenvector analysis of NO_x, HNO_3, and PAN

Equations S1–S12 give explicit formulas for the effective first-order rate constants used in the eigenvector analysis. Values for all rate constants were taken from the IUPAC chemical kinetics database (Atkinson et al., 2006), except for k_{OH+NO_2} which used the results of Dulitz et al. (2018). Formulas for k_{assoc} and k_{dissoc} were taken from LaFranchi et al. (2009). Species marked in bold in the equations were not measured, and concentrations taken from a chemical box model were used instead. S_a is the aerosol surface area concentration, MW_X is the molecular weight of X, and R in Eq. S9 is the gas constant.

$$k_{forward} = \frac{1}{[NO_x]}\left(k_{OH+NO_2}[OH][NO_2] + [RONO_2]\frac{\bar{v}_{RONO_2}\cdot\gamma_{RONO_2}}{4}S_a + [\mathbf{XONO_2}]\frac{\bar{v}_{XONO_2}\cdot\gamma_{XONO_2}}{4}S_a + [\mathbf{N_2O_5}]\frac{\bar{v}_{N_2O_5}\cdot\gamma_{N_2O_5}}{4}S_a\right) \quad (S1)$$

$$k_{backward} = k_{OH+HNO_3}[OH]f_g + j_{gHNO_3}f_g + j_{gHNO_3}EF(1-f_g) \quad (S2)$$

$$k_{removal} = \frac{1}{[NO_x]}\left(\sum_i k_{R_iO_2+NO}[\mathbf{R_iO_2}][NO]\alpha_i\right) \quad (S3)$$

$$k_{dep} = \frac{v_{dep}}{BLH}f_g \quad (S4)$$

$$k_{assoc} = \frac{1}{[NO_x]}\left(k_{CH_3CHO+OH}[CH_3CHO][OH] + j_{Acetone}[Acetone]\right)\beta \quad (S5)$$

$$k_{dissoc} = (k_{PAN} + j_{PAN})\cdot(1-\beta) \quad (S6)$$

$$f_g = \frac{[gHNO_3]}{[gHNO_3]+[pHNO_3]} \quad (S7)$$

$$\beta = \frac{k_{R(O)O_2+NO_2}[NO_2]}{k_{R(O)O_2+NO_2}[NO_2] + k_{R(O)O_2+NO}[NO] + k_{R(O)O_2+HO_2}[HO_2]} \quad (S8)$$

$$\bar{v}_X = \sqrt{\frac{8RT}{\pi\cdot MW_X}} \quad (S9)$$

$$\frac{d[NO_x]}{dt} = -k_{forward}[NO_x] + k_{backward}[HNO_3] - k_{removal}[NO_x] - k_{assoc}[NO_x] + k_{dissoc}[PAN] \quad (S10)$$

$$\frac{d[HNO_3]}{dt} = k_{forward}[NO_x] - k_{backward}[HNO_3] - k_{dep}[HNO_3] \quad (S11)$$

$$\frac{d[PAN]}{dt} = k_{assoc}[NO_x] - k_{dissoc}[PAN] \quad (S12)$$

References

Atkinson, R., Baulch, D. L., Cox, R. A., Crowley, J. N., Hampson, R. F., Hynes, R. G., Jenkin, M. E., Rossi, M. J., Troe, J., and IUPAC Subcommittee: Evaluated kinetic and photochemical data for atmospheric chemistry: Volume II — gas phase reactions of organic species, *Atmos. Chem. Phys.*, *6*(11), 3625–4055, doi: 10.5194/acp-6-3625-2006, **2006**.

Dulitz, K., Amedro, D., Dillon, T. J., Pozzer, A., and Crowley, J. N.: Temperature-(208–318 k) and pressure-(18–696 torr) dependent rate coefficients for the reaction between OH and HNO_3, *Atmos. Chem. Phys.*, *18*(4), 2381–2394, doi: 10.5194/acp-18-2381-2018, **2018**.

LaFranchi, B. W., Wolfe, G. M., Thornton, J. A., Harrold, S. A., Browne, E. C., Min, K. E., Wooldridge, P. J., Gilman, J. B., Kuster, W. C., Goldan, P. D., de Gouw, J. A., McKay, M., Goldstein, A. H., Ren, X., Mao, J., and Cohen, R. C.: Closing the peroxy acetyl nitrate budget: observations of acyl peroxy nitrates (PAN, PPN, and MPAN) during BEARPEX 2007, *Atmos. Chem. Phys.*, *9*(19), 7623–7641, doi: 10.5194/acp-9-7623-2009, **2009**.